Monthly Notices
of the
ROYAL ASTRONOMICAL SOCIETY

MNRAS **466,** 1118–1126 (2017)
Advance Access publication 2016 December 5

doi:10.1093/mnras/stw3153

Two W-subtype contact binaries: GQ Boo and V1367 Tau

Jia Zhang,[1,2⋆] Sheng-Bang Qian,[1,2⋆] Zhong-Tao Han[1,2] and Yue Wu[3⋆]

[1] *Yunnan Observatories, Chinese Academy of Sciences, Kunming 650216, China*
[2] *Key Laboratory of the Structure and Evolution of Celestial Objects, Chinese Academy of Sciences, Kunming 650216, China*
[3] *Key Laboratory of Optical Astronomy, National Astronomical Observatories, Chinese Academy of Sciences, Beijing 100012, China*

Accepted 2016 November 30. Received 2016 November 23; in original form 2016 October 3

ABSTRACT

Two contact binaries, GQ Boo and V1367 Tau, were observed and analysed with a new method to obtain the absolute parameters. The light-curve analysis shows that both of them are obvious W-subtype contact binaries, with much more massive but apparently cooler components ($M_2/M_1 \simeq 2$ and 4, $T_2/T_1 \simeq 0.95$ and 0.94). The orbital periods were studied using the O–C diagrams, and it is thought that the minima timings were heavily affected by the long-standing magnetic activities on the star surface, so the minima timings cannot represent the real period changes. The mass–radius relationships were proposed by the light-curve analysis alone, which is equivalent to the mean density. The density and temperature can determine the other absolute parameters in most of the time. With the almost complete star parameter space provided by PARSEC, approximate masses and radii were obtained ($0.52 \pm 0.08\,M_\odot$ and $1.01 \pm 0.15\,M_\odot$ for GQ Boo, and $0.22 \pm 0.01\,M_\odot$ and $0.92 \pm 0.06\,M_\odot$ for V1367 Tau). The mass–radius relationship is a neglected useful tool to calculate the mass and radius, especially for the detached binaries.

Key words: techniques: photometric – binaries: eclipsing – stars: evolution.

1 INTRODUCTION

The most striking feature of the contact binaries is the shared contact envelop rotating along with the binaries, which is fairly shallow but of nearly uniform temperature. The surface temperatures of the two components are often very close, despite big differences in masses. So an efficient heat transport mechanism is the key to the uniform surface temperature of contact binaries, and the related theories include the angular momentum loss (AML), thermal relaxation oscillation (TRO) (Flannery 1976; Lucy 1976; Robertson & Eggleton 1977), Coriolis force (Zhou & Leung 1990) and differential rotation (Yakut & Eggleton 2005). The latest theory of differential rotation is very natural and inevitable, and it is also applicable to either early- or late-type stars.

The surface temperatures of the two components of a contact binary usually have small (several per cent) but definite difference. On this point Binnendijk (1970) first introduced the classification of A- and W-subtype contact binaries, which correspond to the massive components being hotter and cooler than their companions, respectively. On observations, the majority of A or earlier spectral type contact binaries are found to be A-subtype (Zhou 2016); but for the K or later type contact binaries, all of them are W-subtype (Liu 2014). The A- and W-subtype contact binaries roughly correspond to the early and late spectral types, respectively (Yakut & Eggleton 2005).

Furthermore, many contact binaries have altered their subtypes between A and W in only several years time-span, such as AM Leo (Binnendijk 1969; Hoffmann & Hopp 1982; Derman, Demircan & Dundar 1991), RZ Com (Wilson & Devinney 1973; Xiang & Zhou 2004; Qian & He 2005), TZ Boo (Hoffmann 1978, 1980; Awadalla 1989), AH Cnc (Maceroni, Milano & Russo 1984; Zhang, Zhang & Deng 2005; Qian et al. 2006), SS Ari (Kurochkin 1960; Kim et al. 2003) and FG Hya (Qian & Yang 2005).

The reason for the A-/W-subtype dichotomy is roughly equivalent to the reason for the existence of W-subtype contact binaries, since the situation of A-subtype contact binaries conforms to the intuitive understanding. The rapid altering of the subtypes hints to us that the reason for the W-subtype may be not the stable factors, such as mass, temperature, etc., but the fast time-variable factors, i.e. the magnetic activities, such as spots, flares, etc. And this also explains why the contact binaries are more likely to be W-subtype as the spectral type becomes late, because the magnetic activities are much more intensive in late-type stars.

In this paper, two typical W-subtype contact binaries, GQ Boo and V1367 Tau, are presented with photometrical and spectroscopical data, and analysed with a new method to obtain their absolute parameters without radial velocity data.

The object GQ Boo was first observed by the ROTSE (Robotic Optical Transient Search Experiment) All Sky Surveys and classified as a close binary (Akerlof et al. 2000) with a period of

⋆ E-mail: zhangjia@ynao.ac.cn (JZ); qsb@ynao.ac.cn (S-BQ); wuyue@bao.ac.cn (YW)

0.384 641 d (Blattler & Diethelm 2001). Then many of its minima timings were accumulated, and it was also observed by the Northern Sky Variability Survey (NSVS) (Hoffman, Harrison & McNamara 2009) and Catalina Surveys (Drake et al. 2014). However, no further analysis was carried out on this object so far. In this paper, the first set of high-precision multi-band photometric data is presented and analysed in detail.

The earliest observations of V1367 Tau were released by IBVS (Information Bulletin on Variable Stars) (Menke 2005), and were analysed soon by Yang et al. (2005) who obtained its light-curve solution including mass ratio $M_2/M_1 = 2.975(18)$, temperature ratio $T_2/T_1 = 0.932(4)$ and inclination $i = 66.05(26)$. These data are reanalyzed in the following section (Section 4) but the derived mass ratio is larger at $M_2/M_1 = 4.09(31)$, yet the other parameters do not differ much. In addition, V1367 Tau was reported as displaying coronal activities (Szczygieł et al. 2008).

Section 2 describes the observations and data reduction for the two objects. The binary orbital periods are discussed briefly in Section 3, and the light-curve analysis and the calculation of absolute parameters are presented in Sections 4 and 5. We summarize the paper in Section 6.

2 OBSERVATIONS AND DATA REDUCTION

New photometry of GQ Boo and V1367 Tau was performed using the 1-m telescope of Yunnan Observatories and the 85-cm telescope of Xinglong station, National Astronomical Observatories of China, on 2015 January and 2016 January. The standard Johnson–Cousin–Bessel filters *B, V, R* and *I* along with a high-performance Andor CCD camera were used for both objects. The integration times were 5 to 25 s for GQ Boo and 10 to 50 s for V1367 Tau, depending on filters and weather conditions. All the images were reduced by the Image Reduction and Analysis Facility (IRAF) software in a standard mode with bias and flat corrections. Differential magnitudes were determined between the variable star and a nearby invariable comparison/check star. The typical errors in the final differential magnitudes are 0.01–0.03 mag for GQ Boo and <0.02 mag for V1367 Tau. A total of 2366 points for GQ Boo and 1930 points for V1367 Tau were obtained.

3 THE ORBITAL PERIODS ANALYSIS

All the minima timings of GQ Boo and V1367 Tau were collected and are listed in Table 1 together with our six minima timings. The O–Cs are calculated with the following linear ephemeris, and plotted in Fig. 1.

GQ Boo:

$$\mathrm{Min.I} = 2457\,399.409\,98(14) + 0.384\,639\,624(23)\mathrm{d} \times E,$$

V1367 Tau:

$$\mathrm{Min.I} = 2457\,406.021\,08(10) + 0.347\,677\,962(18)\,\mathrm{d} \times E. \quad (1)$$

It can be seen that for both of the two objects, the dispersions of the points are far beyond their error bars. There are many points that are near to each other in the horizontal axis (time), but are very dispersed in the vertical axis. This indicates that the orbital periods have big jumps within a short time. Take two minima timings from our observations for example: in the right panel of Fig. 1, there are two red points at Epoch -0.1×10000. These two points are the successive secondary and primary light minima in the same observation, i.e. they are only half a period apart, but the deviation of their O–Cs is significant and much bigger than their errors. It is difficult to imagine, within half a cycle, that the period will have such a big sudden change.

We do not think the periods had chaotic and rapid jumps as the O–C diagrams show. The apparent changes are thought to be due to the distortions of the light curves. These two contact binaries are low in surface temperature (5930 and ∼5000 K), so the magnetic activities on the stellar surface should be intensive. This will cause the surface temperature to be not uniform, and make the light curves distorted and asymmetric. Hence the light minimum times deviate from the binary conjunction times, especially for the contact binaries whose light minima are wide and shallow. It is believed that these time deviations may be serious enough for some contact binaries to ruin the intrinsic orbital period variation curve. The two objects, GQ Boo and V1367 Tau, in this paper are such systems.

Therefore, it is believed that the points in Fig. 1 cannot reflect the real changing binary periods. The O–C diagrams show the changes of the light minimum times, rather than the changes of the binary orbital period. A second degree polynomial fitting was carried out for the two objects, but this does not make sense. It can be seen that the fitting curves cannot reflect the variations of the data points. What the O–C diagrams can illustrate is that distortions of the light curve often occurred in the past 10 years, which also indirectly indicates the long-term existence of the magnetic activities.

The distortion of the light curves not only affects the period analysis, but also affects the following light-curve analysis. This requires us to judge the reliability of the analysis results (see the next section).

4 THE BINARY LIGHT-CURVE ANALYSIS

4.1 The temperatures of the binary components

The temperatures of the two contact binaries were measured from spectral data (GQ Boo) or colour indices (V1367 Tau). Two spectra of GQ Boo were provided by the Guoshoujing Telescope (the Large Sky Area Multi-Object Fibre Spectroscopic Telescope, LAMOST), and one of them was observed on 2012 March 6 and is plotted in Fig. 2. The two spectra were analysed by ULYSS (Universite de Lyon Spectroscopic analysis Software; Koleva et al. 2009; Wu et al. 2011a) which was already successfully implemented on the LAMOST stellar parameter pipeline [LASP; Wu et al. (2011b, 2014); section 4.4 of Luo et al. (2015)]. It automatically derived the stellar atmospheric parameters via full spectral fitting between the observation and the model spectrum. The model spectrum is generated by an interpolator by using the ELODIE library (Prugniel & Soubiran 2001; Prugniel et al. 2007) as reference. The fitting is displayed in Fig. 2 within the wavelength range 3900–6800 A. The analysis in this paper was optimized especially for the binarity of GQ Boo, and derived atmosphere parameters were $T = 5930(\pm 30)$ K, $\log g = 4.2(\pm0.4)$ cm s^{-2} and [Fe/H] = 0.02(±0.2).

The temperature of V1367 Tau was estimated based on the colour indices. The Johnson *B* (11.964 ± 0.15) and *V* (11.135 ± 0.142), and Sloan *g*' (11.527 ± 0.178), *r*' (10.852 ± 0.127) and *i*'(10.632 ± 0.171) band magnitudes from AAVSO Photometric All Sky Survey (APASS; Henden et al. 2016), and *J* (9.550 ± 0.023), *H* (9.142 ± 0.030) and K_s (9.083 ± 0.021) band magnitudes from Two Micron All-Sky Survey (2MASS; Cutri et al. 2003) were used to calculate the colour indices. However, the band magnitudes need to be extinction corrected first. The 'Rayleigh–Jeans Colour Excess' (RJCE) method (Majewski, Zasowski & Nidever 2011) was used to calculate extinction of K_s band using the formula

Table 1. The minima timings of GQ Boo and V1367 Tau.

GQ Boo				V1367 Tau			
HJD	Error	Method	Reference	HJD	Error	Method	Reference
51274.7820	0.001?	CCD	Paschke, Anton.[a]	53683.4307	0.0014	CCD	Diethelm (2006)
51996.5626	0.0011	CCD	Blaettler (2012)	53683.6080	0.0010	CCD	Diethelm (2006)
52001.3714	0.0006	CCD	Blaettler (2012)	53686.3878	0.0012	CCD	Diethelm (2006)
52001.5659	0.0010	CCD	Blaettler (2012)	53686.5598	0.0009	CCD	Diethelm (2006)
52022.3460	0.003	CCD	Blaettler (2012)	53694.3846	0.0003	CCD	Diethelm (2006)
52022.5294	0.0017	CCD	Blaettler (2012)	53694.5591	0.0013	CCD	Diethelm (2006)
52041.5649	0.0009	CCD	Blaettler (2012)	53705.3330	0.0030	CCD	Diethelm (2006)
52367.3593	0.0015	CCD	Blaettler (2012)	53705.5131	0.0008	CCD	Diethelm (2006)
52699.8770	0.001?	CCD	Paschke, Anton.[a]	53705.6839	0.001?	CCD	Blaettler, Ernst.[a]
52763.3470	0.003	CCD	Diethelm (2003)	53705.6854	0.0009	CCD	Diethelm (2006)
52839.5053	0.0012	CCD	Diethelm (2004)	53741.3209	0.0004	CCD	Diethelm (2006)
53081.4510	0.002	CCD	Diethelm (2004)	53741.4933	0.0005	CCD	Diethelm (2006)
53445.5100	0.002	CCD	Diethelm (2005)	53760.2680	0.0015	CCD	Diethelm (2006)
53863.4199	0.0009	CCD	Moschner (2007)	53760.4452	0.0009	CCD	Diethelm (2006)
53936.4930	0.004	CCD	Diethelm (2007)	53768.2560	0.0030	CCD	Diethelm (2006)
54161.9020	0.001	CCD	Nelson (2008)	53768.4418	0.0007	CCD	Diethelm (2006)
54186.5145	0.0031	CCD	Hubscher (2007)	54130.3697	0.0005	CCD	Diethelm (2007)
54197.4751	0.0014	CCD	Diethelm (2007)	54849.7205	0.0005	CCD	Diethelm (2009)
54201.5208	0.0012	CCD	Hubscher (2007)	55153.9349	0.0004	CCD	Diethelm (2010)
54213.4402	0.0022	CCD	Hubscher (2007)	55517.9585	0.0004	CCD	Diethelm (2011a)
54520.9612	0.0003	CCD	Nelson (2009)	55528.5606	0.0003	CCD	Demircan (2012)
54565.1953	0.001?	CCD	Nakajima (2009)	55595.3150	0.0002	CCD	Aydin (2012)
54570.3868	0.0011	CCD	Hubscher, Steinbach & Walter (2009)	55873.6325	0.0005	CCD	Gokay (2013)
54570.5796	0.0017	CCD	Hubscher et al. (2009)	55888.9302	0.0006	CCD	Diethelm (2012a)
54908.4847	0.0002	CCD	Hubscher et al. (2010)	55901.4483	0.0008	CCD	Okan (2013)
54933.4866	0.0008	CCD	Hubscher et al. (2010)	55901.6194	0.0007	CCD	Okan (2013)
54945.4105	0.0002	CCD	Hubscher et al. (2010)	56313.6167	0.0004	CCD	Diethelm (2013)
54965.7952	0.0006	CCD	Diethelm (2009)	57028.9638	0.0002	CCD	this paper
54968.4890	0.0005	CCD	Hubscher et al. (2010)	57029.1387	0.0002	CCD	this paper
55015.4080	0.004	CCD	Blaettler (2010)	57388.2874	0.001?	CCD	Itoh (2016)
55315.4348	0.0039	CCD	Huebscher & Monninger (2011)	57406.0205	0.0002	CCD	this paper
55339.6680	0.001?	CCD	Paschke, Anton.[a]	57406.1945	0.0002	CCD	this paper
55398.5129	0.0010	CCD	Blaettler (2011)				
55643.9183	0.0007	CCD	Diethelm (2011b)				
55654.4942	0.0025	CCD	Hubscher, Lehmann & Walter (2012)				
55667.3784	0.0003	CCD	Hubscher et al. (2012)				
55697.7608	0.0008	CCD	Diethelm (2011b)				
56009.5149	0.0028	CCD	Agerer (2013)				
56023.9431	0.0008	CCD	Diethelm (2012b)				
56089.7139	0.0004	CCD	Diethelm (2012b)				
57399.4081	0.00017	CCD	This paper				
57400.3701	0.00051	CCD	This paper				

Notes. [a]The observer's name was taken from O–C gateway (http://var2.astro.cz/ocgate/).
[?]The error cannot be obtained from the data source. Here we artificially set it to be a typical CCD measurement error 0.001 d.
All the referenced data were collected with the help of the website O–C gateway (http://var2.astro.cz/ocgate/).

$A(K_s) = 0.987097 \times (H - W2 - 0.08)$ (private communication with Huang Y. based on Yuan, Liu & Xiang 2013), where $W2$ (9.065 ± 0.020) is band 2 (4.6 micrometers) of Wide-field Infrared Survey Explorer (WISE). Then the extinctions of other bands were calculated with the extinction coefficients derived by Yuan et al. (2013). Finally, the colour indices after reddening corrections were calculated and used to estimate the temperatures, using the colour–temperature calibrations by Huang et al. (2015). A total of eight colour indices were used to get a rough temperature $T = 5000(\pm 300)$ K.

Only one temperature was obtained from the observations for the binary systems, which have two components with different temperatures. Generally, the single observed temperature was assigned to the luminous component, because it dominates the light. This is an acceptable assumption for light-curve analysis, because the light curves constrain the temperature ratio quite strongly but not the individual temperatures (Yakut & Eggleton 2005), and an example from Zhang & Qian (2013) shows that a huge 5800 K change of primary temperature does not affect the mass ratio. However in this paper, a relatively more accurate primary temperature was obtained based on an assumption. The assumption is that the single measured temperature T (no matter from spectra or colour index) follows the Stefan–Boltzmann law on the whole binary system, i.e. $L = S\sigma T^4$, where L and S are the total luminosity and total surface area of the whole binary system, respectively, and T is the single measured temperature, and σ is the Stefan–Boltzmann constant.

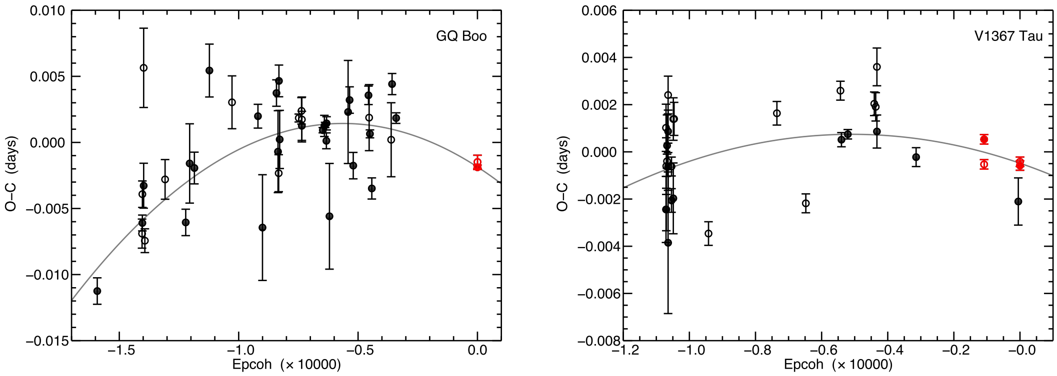

Figure 1. The O–C diagram of GQ Boo (left) and V1367 Tau (right). The filled and open circles stand for the primary and secondary minima, respectively. The red points are from our observations. The curves stand for the second degree polynomial fittings. Note: one point of V1367 Tau, corresponding to 2453 768.2560(0.0030), is not shown and fitted due to its excessively large scatter.

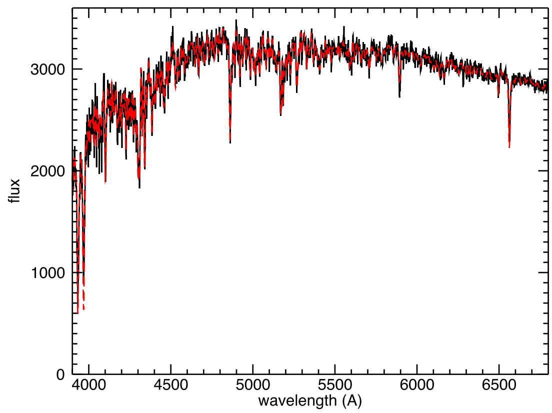

Figure 2. The spectra of GQ Boo from LAMOST. The black solid line and red dashed line stand for the observations and fitting.

Based on the above assumption, two equations can be written:

$$L = S\sigma T^4 = (4\pi R_1^2 + 4\pi R_2^2)\sigma T^4,$$
$$L = L_1 + L_2 = 4\pi R_1^2\sigma T_1^4 + 4\pi R_2^2\sigma T_2^4. \quad (2)$$

$L_{1,2}$, $R_{1,2}$ and $T_{1,2}$ are the luminosities, radii and temperatures of the binary components, respectively. Combined with the relative radii $r_{1,\,2}$ ($=R_{1,\,2}/A$, and A is semimajor axis) and T_2/T_1 obtained from the light-curve analysis (see Table 2), T_1 and T_2 can be worked out.[1] However, the light-curve analysis first needs the primary temperature as an input parameter. Actually, we did the calculation in an iterative way. First, the light curves were analysed with the single measured temperature as the primary temperature, and then $r_{1,\,2}$ and T_2/T_1 were obtained. Secondly, the more accurate primary temperature was calculated using equation (2). Then the light curves were analysed again with the more accurate primary temperature. Because the changes in primary temperature have little effect on other output parameters, the second time results from the light-curve analysis are very close to those of the first time. If the new $r_{1,\,2}$ and T_2/T_1 were used to calculate a more accurate primary temperature again, the new primary temperature will not have a big difference from the previous value [specifically, the differences are 13 K and 23 K (or 0.2 and 0.4 per cent) for GQ Boo and V1367 Tau, respectively]. So sufficiently accurate primary temperatures were obtained based on the assumption of the Stefan–Boltzmann law on the whole binary system, and they are listed in Table 2.

4.2 The light-curve analyses

The observed light curves were folded to the phase curves based on their orbital periods and the current light minima timings, and then the phase curves were binned to make the data points distributed evenly in phase. These binned data were analysed using the Wilson–Devinney program (Wilson & Devinney 1971; Wilson 1979, 1990, 2008, 2012; Van Hamme & Wilson 2007; Wilson, Van Hamme & Terrell 2010), which is a model that can generate binary light curves theoretically and fit the observed light curves to get the relative parameters, such as mass ratio, relative radius, temperature ratio etc.

The mass ratio is a very important parameter. In order to obtain the mass ratio as reliable as possible, a common technique called mass ratio search (q-search) was used. This technique is to fit the light curves with mass ratios fixed at a series of given values, so a series of corresponding solutions are obtained. Then the solution with the best fit was selected to fit the light curves finally, with the mass ratio set to be adjustable, to get the final solution.

In the fitting, the primary temperatures were fixed at the values calculated by the method described in Section 4.1. The exponents g in the bolometric gravity brightening law and the bolometric albedos A for reflection heating and re-radiation are fixed at $g = 0.32$ and $A = 0.5$ for both components, because the contact envelops are probably convective due to their low temperatures ($\sim$5930 K for GQ Boo and $\sim$5000 K for V1367 Tau). The logarithmic law for limb darkening was used, and the coefficients are internally calculated in the program as a function of temperature $T_{\rm eff}$, surface gravity $\log g$ and metallicity $[M/H]$ based on the Van Hamme (1993) table. For GQ Boo, $\log g$[2] and $[M/H]$ derived from the spectra were applied, and for V1367 Tau, the rough guessed values were used ($\log g \approx 4.3$ and $[M/H] \approx -0.10$). We need not be worried about the inaccuracies of the $\log g$ and $[M/H]$ because their effects on the light curves are quite small and hardly affect the other output parameters.

[1] $R_{1,\,2}$ can be replaced by $r_{1,\,2}$ in the simultaneous equations, and T_2 can be substituted by $(T_2/T_1) \times T_1$. So the only unknown variable T_1 can be worked out.

[2] The $\log g$ is not a direct input parameter in the program, but calculated indirectly from the period and the semimajor axis. So we adjust the semimajor axis to match the measured value approximately.

Table 2. The light-curve solutions of GQ Boo and V1367 Tau.

Parameters	GQ Boo (data of 2016) (Recommended)	V1367 Tau (mean)^{a} (Recommended)	V1367 Tau (data of 2015)	V1367 Tau (data of 2016)	V1367 Tau (data from Yang et al. (2005))
Mode	Contact binary	Contact binary	Contact binary	Contact binary	contact binary
Orbital inclination i (◯)	62.860(91)	66.78(33)	64.48(23)	66.85(22)	66.71(62)
Mass ratio m_2/m_1	1.952(37)	4.25(17)	5.62(15)	4.40(12)	4.09(31)
Primary temperature $T_1{}^{b}$ (K)	6129 (fixed)	5220 (fixed)	5220 (fixed)	5220 (fixed)	5220 (fixed)
Temperature ratio T_2/T_1	0.9452(18)	0.9422(26)	0.8943(21)	0.9404(17)	0.9439(44)
Luminosity ratio $L_1/(L_1+L_2)$ in band B	0.4370(36)	–	0.3431(43)	0.2962(40)	–
Luminosity ratio $L_2/(L_1+L_2)$ in band B	0.5630(36)	–	0.6569(43)	0.7038(40)	–
Luminosity ratio $L_1/(L_1+L_2)$ in band V	0.4149(33)	0.2811(58)	0.3058(39)	0.2771(38)	0.285(11)
Luminosity ratio $L_2/(L_1+L_2)$ in band V	0.5851(33)	0.7190(58)	0.6942(39)	0.7229(38)	0.715(11)
Luminosity ratio $L_1/(L_1+L_2)$ in band Rc	0.4049(32)	0.2688(58)	0.2793(36)	0.2645(36)	0.273(11)
Luminosity ratio $L_2/(L_1+L_2)$ in band Rc	0.5951(32)	0.7313(58)	0.7207(36)	0.7355(36)	0.727(11)
Luminosity ratio $L_1/(L_1+L_2)$ in band Ic	0.3971(31)	–	0.2625(35)	0.2560(35)	–
Luminosity ratio $L_2/(L_1+L_2)$ in band Ic	0.6029(31)	–	0.7375(35)	0.7440(35)	–
Modified dimensionless surface potential of star 1	5.100(51)	8.07(20)	9.63(18)	8.25(15)	7.88(38)
Modified dimensionless surface potential of star 2	5.100(51)	8.07(20)	9.63(18)	8.25(15)	7.88(38)
Fillout factor f^{c}	0.140(86)	0.25(33)	0.46(28)	0.26(23)	0.24(61)
Radius of star 1 (relative to semimajor axis) in pole direction	0.3095(15)	0.2548(29)	0.2385(16)	0.2519(19)	0.2577(54)
Radius of star 2 (relative to semimajor axis) in pole direction	0.4179(60)	0.475(13)	0.5139(93)	0.4804(89)	0.470(25)
Radius of star 1 (relative to semimajor axis) in side direction	0.3242(16)	0.2665(30)	0.2501(17)	0.2634(20)	0.2695(57)
Radius of star 2 (relative to semimajor axis) in side direction	0.4449(79)	0.515(19)	0.568(15)	0.521(13)	0.508(35)
Radius of star 1 (relative to semimajor axis) in back direction	0.3617(16)	0.3075(31)	0.2988(17)	0.3046(21)	0.3104(58)
Radius of star 2 (relative to semimajor axis) in back direction	0.476(11)	0.539(24)	0.596(19)	0.546(17)	0.532(45)
Equal-volume radius of star 1 (relative to semimajor axis) r_1	0.33336(89)	0.2760(18)	0.26492(98)	0.2736(12)	0.2783(33)
Equal-volume radius of star 2 (relative to semimajor axis) r_2	0.4499(49)	0.521(11)	0.5524(83)	0.5243(74)	0.518(20)
Radius ratio R_2/R_1	1.350(15)	1.889(39)	2.085(33)	1.917(29)	1.860(76)

Notes. ^{a}This solution is the mean value of the last two column solutions, i.e. the solution based on data of 2016 and data from Yang et al. (2005).
^{b}The primary temperatures were obtained by the method described in Section 4.1.
$^{c}f = (\Omega_{\rm star} - \Omega_{\rm inner})/(\Omega_{\rm outer} - \Omega_{\rm inner})$, where $\Omega_{\rm star}$, $\Omega_{\rm inner}$ and $\Omega_{\rm outer}$ are the modified dimensionless potential of star surface, inner Roche lobe and outer Roche lobe, respectively.
Note. The two digital numbers in the parentheses are the errors on the last two bits of the data.

The solutions are shown in Figs 3 and 4 and are listed in Table 2. The third column (V1367 Tau (mean)) of Table 2 is the mean value of the last two columns. For V1367 Tau, the three solutions have obvious differences, so their reliability need to be judged. A discussion on the reliability is given in the next section.

4.3 The reliability of the light-curve solutions

If the binary light curves are changeless with time, the light-curve solutions for data observed at different times should be the same. However, the light curves are always changing, more or less. The reasons for the changes could be various, but the most common reason is the magnetic activities on the star surface, especially for the low-temperature contact binaries, just like the two objects here. The magnetic activities, such as spots and flares, will distort the light curves in a random way. Therefore, the analysis solutions may be different for observations at different times.

One question arises, if the solutions change over time, how to choose the correct one, or the best one? Technically, maybe there are two rulers can be used to measure the reliability of the solution. One is the degree of symmetry of the light curves. If the light curves are symmetric, the distortions by the magnetic activities are probably very small, so the solution will indicate the intrinsic binary geometric structure. Conversely, if the light curves are very asymmetric, the distortions may change the intrinsic solution a lot. Therefore, the degree of symmetry can be used to measure the reliability. The other reliability ruler is the degree of sharpness of the q-search curve bottom. The sharper the q-search curve bottom, the smaller the uncertainty of the mass ratio, and the more reliable the corresponding solution.

Based on the two rulers proposed above, the reliability of light-curve solutions of the two objects, GQ Boo and V1367 Tau, will be discussed. For GQ Boo, the light curves are generally symmetric with only local scatter at phase around 0.5 (see the lower panel of Fig. 3). The bottom of the q-search curve is sharp (In other words, a rough position of the minimum point can be found easily, and the scatter of the points will not obscure the minimum considerably; quantitatively, the minimum should be between 1.9 and 2.1.). Therefore, it is believed that the solution of GQ Boo is generally reliable.

For V1367 Tau, all the light curves from the three observations are generally symmetric but with O'Connell effects on the first two observations (see the lower panels of Fig. 4). The q-search curves are not as sharp as for GQ Boo. For the data observed in 2015 (left upper panel of Fig. 4), the q-search curve has a wide bottom (visually, all the points from 4.6 to 5.6 could be at the bottom). So the mass ratio of 5.62(0.15) is likely to be unreliable. Because of this situation, a second observation of V1367 Tau was carried out in 2016 January, and the results are shown in the middle panels of Fig. 4. It can be seen that the width of the q-search bottom obviously narrowed (compared to the data of 2015), but the bottom is still about 0.5 width (visually, from 3.9 to 4.4). So the mass ratio 4.40(0.12) may have an uncertainty of 0.5. Besides our observations, the data from Yang et al. (2005) were also collected and analysed in the same

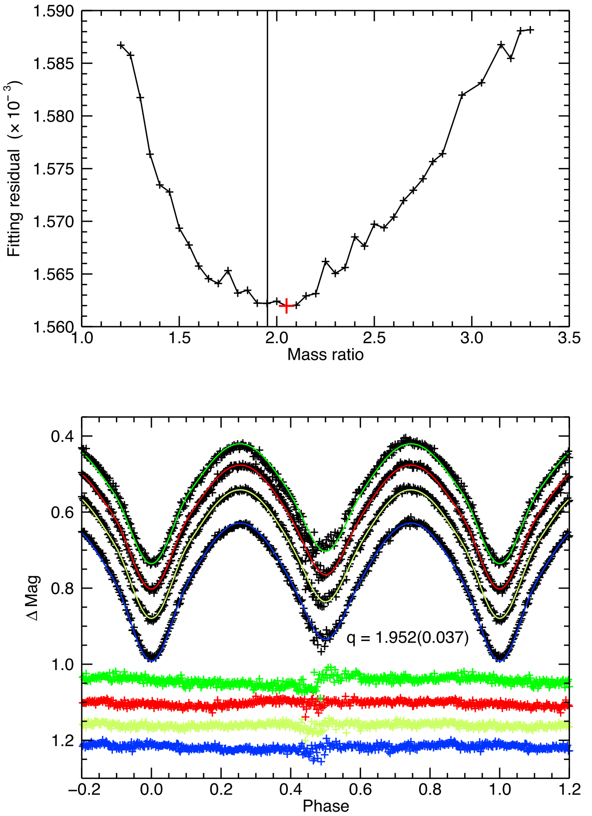

Figure 3. Upper: the q-search diagram of GQ Boo with the lowest point marked in red. The vertical line represents the position of the final fitted mass ratio after it is set to be adjustable. Lower: the observed light curves (black points) of GQ Boo with the fitting lines (in colour) and their corresponding fitting residuals (the horizontal colour points located in the lower part). The blue, yellow, red and green in the lower panel stand for band *B*, *V*, *R* and *I*, respectively.

way, and the results are shown in the right panels of Fig. 4. It can be seen that q-search bottom is clearly sharp around 4.1. In addition, the light curves are symmetric without the O'Connell effect. So, it is thought that the mass ratio of 4.09(0.31) may be better than 4.40(0.12).

Besides the mass ratio, the other output parameters also need to be measured for their reliability. However, the other parameters [$r_{1,2}$, T_2/T_1 and $L_1/(L_1 + L_2)$ etc.] do not change much with the mass ratio. It can be found from the three solutions of V1367 Tau in Table 2, the parameters except mass ratio do not differ much from each other. The differences of parameters between the solutions for data of 2016 and Yang et al. (2005) are almost smaller than their error ranges. Even when we compare the solutions for data of 2015 and 2016, the differences of most parameters do not exceed 10 per cent, despite the 28 per cent difference between the mass ratios. This indicates that the parameters except mass ratio are generally stable, so they are generally reliable.

In summary, the solution of GQ Boo and the mean solution of V1367 Tau (the third column of Table 3) are recommended. The errors of the parameters may be somewhat underestimated, but it is believed that real errors will not exceed 10 per cent for mass ratio and 5 per cent for other parameters.

Nevertheless, it is well known that the mass ratios based only on light curves are very uncertain compared to those of radial velocities. So the mass ratios here need confirmation from radial velocities. Recently, Rucinski (2015) concluded that the well-known contact binary AW UMa studied by light curves is arguably semidetached, based on the high-resolution spectra. This indicates that the light-curve analysis can be wrong, not only on the mass ratio, but also in the models.

5 THE ABSOLUTE PARAMETERS OF THE BINARY COMPONENTS BY A NEW METHOD

The light-curve analysis can provide not only the relative parameters but also a relationship between the star mass and radius for each component star. The light-curve analysis provides the mass ratio M_2/M_1, i.e. $M_{1,2}/M$, and the radius relative to the semimajor axis $R_{1,2}/A$, where M and A are the total mass and semimajor axis of a binary system, respectively. Kepler's law can be regarded as a relationship between M and A since the accurate orbital period is known. Combined with the relative parameters $M_{1,2}/M$ and $R_{1,2}/A$ provided by the light-curve analysis, the relationships between $M_{1,2}$ and $R_{1,2}$ can be obtained. For the two contact binary objects here, the relationships are:

the massive component of GQ Boo:

$$1.519(74)\frac{M_2}{\mathrm{M}_\odot} = \left(\frac{R_2}{\mathrm{R}_\odot}\right)^3;$$

the massive component of V1367 Tau:

$$1.68(51)\frac{M_2}{\mathrm{M}_\odot} = \left(\frac{R_2}{\mathrm{R}_\odot}\right)^3. \tag{3}$$

The mass–radius relationship can be regarded as a limitation on the absolute parameters. In addition, there is another limitation, i.e. the effective temperature (and a rough metallicity for GQ Boo). These two limitations can match out the absolute star parameters approximately in a complete star parameter space. The complete star parameters can be provided by the evolutionary code PARSEC, which can calculate stellar evolution[3] for almost all the initial stellar masses ($0.1 < M/\mathrm{M}_\odot < 350$) and ages [$6.6 < \log(t/\mathrm{yr}) < 10.13$] at a given metallicity.

From all the star parameters by PARSEC, the stars with a temperature of 5593–5993 K and metallicity $Z = 0.010$–0.023 were selected for GQ Boo. This temperature range is the massive component's temperature 5793 K with 200 K error, and the metallicity range is measured from the spectral data. All the selected stars are plotted in the M–R diagram along with the curve described by equation (3), and the single coincidence region is shown in the left panel of Fig. 5, i.e. the black plus points in the belt area surrounded by the green lines.

For V1367 Tau, the temperatures and metallicity of the selected stars are 4518–5318 K and $Z = 0.0001$–0.0700, respectively. The temperature of the massive component of V1367 Tau was calculated as 4918 K, and a 400 K error was added to make the range 4518–5318 K. Because there are no spectral data to measure the metallicity, so the stars with almost all possible metallicity $Z = 0.0001$–0.0700 were selected. The selected stars around the single coincidence region are shown in the right panel of Fig. 5.

The massive components are probably located in the area of the black points enclosed by the green lines, and then the absolute parameters are read out from Fig. 5 approximately, and listed in Table 3. Star 2 was the massive component, and the parameters of

[3] The evolutional data can be obtained from http://stev.oapd.inaf.it/cgi-bin/cmd.

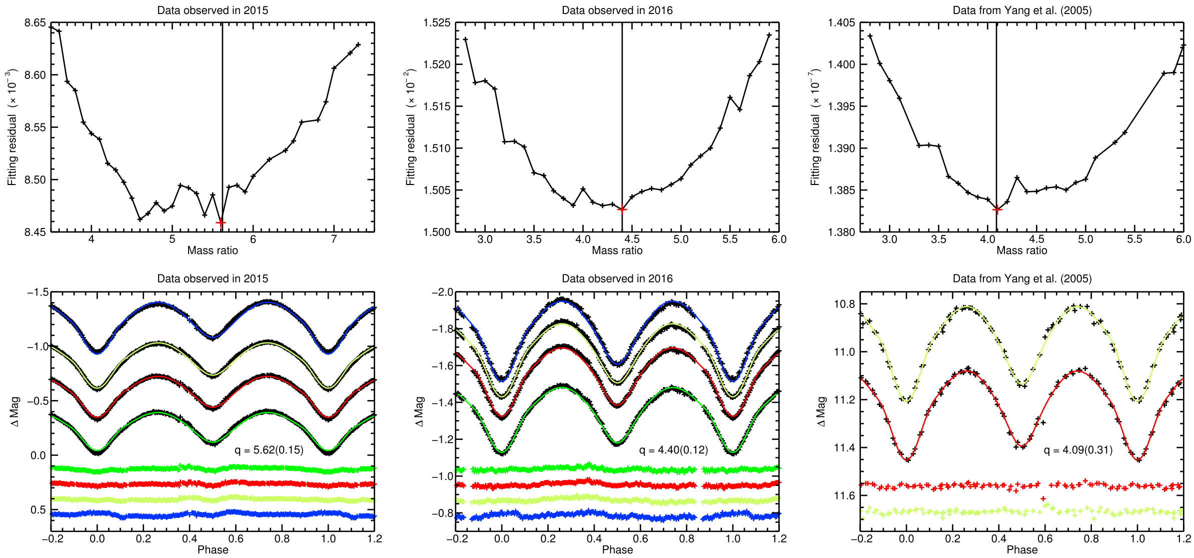

Figure 4. The same as Fig. 3 but for V1367 Tau. The left, middle and right panels stand for the data observed in 2015 January, 2016 January and data from Yang et al. (2005), respectively.

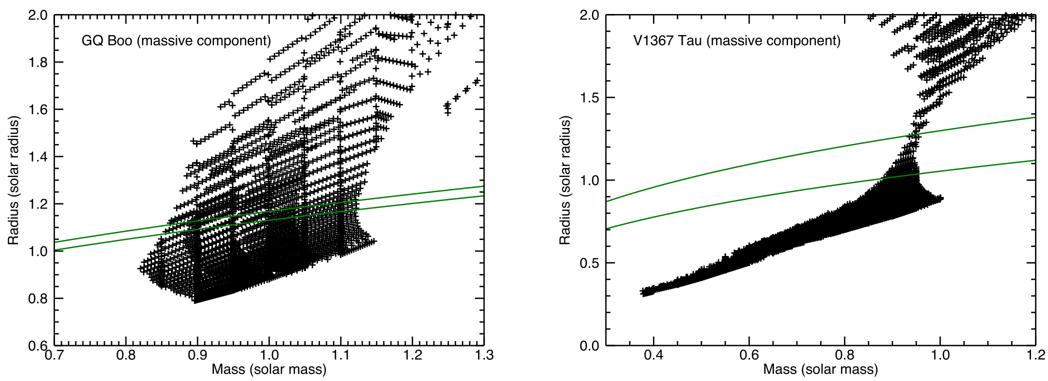

Figure 5. The stellar M–R diagram with the M–R relationship for GQ Boo (left) and V1367 Tau (right). The black plus points represent the stars generated by the PARSEC program, and the areas enclosed by the two green lines are the M–R relationship described by equation (3). The range of temperatures and metallicity Z of the black points are 5593–5993 K and $Z = 0.010$–0.023 for GQ Boo, respectively, and 4518–5318 K and $Z = 0.0001$–0.0700 for V1367 Tau, respectively. See the text for other input parameters of the PARSEC program.

Table 3. The absolute parameters of GQ Boo and V1367 Tau.

Parameters	GQ Boo	V1367 Tau
M_1 ($M_\odot$)	0.52 ± 0.08	0.22 ± 0.01
M_2 ($M_\odot$)	1.01 ± 0.15	0.92 ± 0.06
R_1 ($R_\odot$)	0.85 ± 0.05	0.59 ± 0.10
R_2 ($R_\odot$)	1.15 ± 0.07	1.10 ± 0.20
$\rho_1(\rho_\odot)^a$	0.829 ± 0.011	0.956 ± 0.044
$\rho_2(\rho_\odot)^a$	0.659 ± 0.032	0.60 ± 0.19
T_1 (K)	6129 ± 200	5220 ± 400
T_2 (K)	5793 ± 200	4918 ± 400
Period (d)	0.384 639 624(23)	0.347 677 962(18)

Note. [a]The mean densities $M/(\frac{4}{3}\pi R^3)$ in solar unit of 1410.040 842 Kg/m^3. The densities are derived from light-curve analysis (see equation 3).

star 1 were calculated from star 2 and the relative parameters in Table 2.

There are three points that need to be stated. First, why were the massive components used to match the absolute parameters? Because the less massive components were heavily affected by their massive companions, and their surface temperatures and radii are far from those of the single star with the same mass. Thus, the massive components are more suitable for matching the absolute parameters.

Secondly, although the massive components are more suitable, they still suffer deviations from a single star with the same mass. For the two contact binaries here, the mass ratios are ∼2 (GQ Boo) and ∼4 (V1367 Tau). So it can be inferred that almost all the radiation of the whole binary systems come from the nuclear reaction of the massive components. However, there is ∼40 per cent (GQ Boo) and ∼30 per cent (V1367 Tau) of the luminosity of the binary system radiated from the less massive stars. If the massive stars become single stars, they will be brighter, larger and hotter. This will bring deviations in estimating the masses based on the single star evolutionary model. However, it is thought that the deviations are already covered by the big errors in Table 3.

Thirdly, the reality of the evolutionary model and the input parameters has effects on the results in Table 3. The input parameters of PARSEC include but are not limited to the helium abundance ($Y = 0.2485 + 1.78Z$), the mixing-length parameter in the convection zone $\alpha_{\rm MLT} = 1.74$, and the coefficient of Reimers mass-loss formula $\eta_{\rm Reimers} = 0.2$. The inaccuracy of the input parameters will lead to further uncertainty in the results. However, the uncertainties caused by the evolutionary model are very minor compared to the big errors in the atmosphere parameters.

6 SUMMARY AND CONCLUSION

Two W-subtype contact binaries, GQ Boo and V1367 Tau, were studied photometrically. The light curves were analysed using the Wilson–Devinney program, and the relative parameters were obtained. The results showed that the two objects are obvious W-subtype contact binaries, with the much more massive but apparently cooler components. The reason for the W-subtype contact binaries and the changes on the light curves (and also the scatters on the O–C diagrams) are guessed to be the same, i.e. the time-variable magnetic activities on the star surface.

The orbital periods were also discussed with all collected minima timings. It is thought that the minima timings were heavily affected by the magnetic activities on the star surface, so the minima timings cannot reflect the real orbital period changes. The chaotic O–C diagrams just indicate the longstanding magnetic activities.

Based only on the light-curve analysis, the mass–radius relationship of the binary components was proposed, namely, the mass is proportional to the cubed radius. In other words, the light curves can provide the mean density of the binary components. If the light curves have decent quality and multiple bands, the error of the density can be rather small. The binary light curves can not only provide relative parameters, such as mass ratio, relative radius, temperature ratio and luminosity ratio, but can also provide an absolute parameter, i.e. the mean density. This is a useful parameter but has been neglected.

Using the density from the light-curve analysis, the absolute parameters are estimated with a new method. The program PARSEC provided the parameters of almost all the possible stars, with initial stellar masses $0.1 < M/\,\mathrm{M}_{\odot} < 350$ at ages $6.6 < \log\,(t/\mathrm{yr}) < 10.13$. The density and the surface temperature (and metallicity) can determine a star exclusively for most of the time. The massive component's masses and radii of the two objects were estimated by this method, i.e. choosing the stars with similar temperature and density in the large star parameter space, and the less massive components were calculated by the relative parameters from light-curve analysis. The biggest danger of this method is the difference between the contact binary component and the single star with the same mass, so the errors of the absolute parameters cannot be small. If this method is applied to detached binaries, the accuracy can be high.

ACKNOWLEDGEMENTS

We thank Peter P. Eggleton for his great help both in astrophysics and regarding the language of article. New observations were obtained with the 1-m telescope at Yunnan Observatories and the 85-cm telescope at Xinglong station, National Astronomical Observatories. We acknowledge the support of the staff of Xinglong 85- cm telescope. This work was partially supported by the Open Project Programme of Key Laboratory of Optical Astronomy, National Astronomical Observatories, Chinese Academy of Sciences. The spectral data were provided by Guoshoujing Telescope (LAMOST) which is a National Major Scientific Project built by the Chinese Academy of Sciences. Funding for the project has been provided by the National Development and Reform Commission. LAMOST is operated and managed by the National Astronomical Observatories, Chinese Academy of Sciences.

This work is partly supported by the West Light Foundation of The Chinese Academy of Sciences, Yunnan Natural Science Foundation (Y5XB071001), Guangdong Provincial Engineering Technology Research Center for Data Science, Chinese Natural Science Foundation (No. 11133007, 11325315, U1631108 and 11403056), the Key Research Programme of the Chinese Academy of Sciences (grant No. KGZD-EW-603), the Science Foundation of Yunnan Province (No. 2012HC011), and by the Strategic Priority Research Programme 'The Emergence of Cosmological Structures' of the Chinese Academy of Sciences (No.XDB09010202).

REFERENCES

Agerer F., 2013, Information Bulletin on Variable Stars, 6048
Akerlof C. et al., 2000, AJ, 119, 1901
Awadalla N. S., 1989, Ap&SS, 162, 211
Aydin E., 2012, Information Bulletin on Variable Stars, 6039
Binnendijk L., 1969, AJ, 74, 1031
Binnendijk L., 1970, Vistas Astron., 12, 217
Blaettler E., 2001, BBSAG Bulletins Nr. 125
Blaettler E., 2002, BBSAG Bulletins Nr. 128
Blaettler E., 2010, Information Bulletin on Variable Stars, 5920
Blaettler E., 2011, Information Bulletin on Variable Stars, 5960
Blattler E., Diethelm R., 2001, Information Bulletin on Variable Stars, 5125, 1
Cutri R. M. et al., 2003, VizieR Online Data Catalog, 2246
Demircan Y., 2012, Information Bulletin on Variable Stars, 6039
Derman E., Demircan O., Dundar H., 1991, Information Bulletin on Variable Stars, 3630, 1
Diethelm R., 2003, Information Bulletin on Variable Stars, 5438, 1
Diethelm R., 2004, Information Bulletin on Variable Stars, 5543, 1
Diethelm R., 2005, Information Bulletin on Variable Stars, 5653, 1
Diethelm R., 2006, Information Bulletin on Variable Stars, 5713, 1
Diethelm R., 2007, Information Bulletin on Variable Stars, 5781, 1
Diethelm R, 2009, Information Bulletin on Variable Stars, 5894
Diethelm R, 2010, Information Bulletin on Variable Stars, 5920
Diethelm R., 2011a, Information Bulletin on Variable Stars, 5960
Diethelm R., 2011b, Information Bulletin on Variable Stars, 5992
Diethelm R., 2012a, Information Bulletin on Variable Stars, 6011
Diethelm R., 2012b, Information Bulletin on Variable Stars, 6029
Diethelm R., 2013, Information Bulletin on Variable Stars, 6063
Drake A. J. et al., 2014, ApJS, 213, 9
Flannery B. P., 1976, ApJ, 205, 217
Gokay G., 2013, Information Bulletin on Variable Stars, 6075
Henden A. A., Templeton M., Terrell D., Smith T. C., Levine S., Welch D., 2016, VizieR Online Data Catalog, 2336
Hoffmann M., 1978, Information Bulletin on Variable Stars, 1487, 1
Hoffmann M., 1980, A&AS, 40, 263
Hoffmann M., Hopp U., 1982, Ap&SS, 83, 391
Hoffman D. I., Harrison T. E., McNamara B. J., 2009, AJ, 138, 466
Huang Y., Liu X.-W., Yuan H.-B., Xiang M.-S., Chen B.-Q., Zhang H.-W., 2015, MNRAS, 454, 2863
Hubscher J., 2007, Information Bulletin on Variable Stars, 5802, 1
Hubscher J., Steinbach H.-M., Walter F., 2009, Information Bulletin on Variable Stars, 5874, 1
Hubscher J., Lehmann P. B., Monninger G., Steinbach H.-M., Walter F., 2010, Information Bulletin on Variable Stars, 5918, 1
Hubscher J., Lehmann P. B., Walter F., 2012, Information Bulletin on Variable Stars, 6010, 1
Huebscher J., Monninger G., 2011, Berliner Arbeitsgemeinschaft fuer Veraenderliche Sterne-Mitteilungen, 214, 1
Itoh H., 2016, Variable Star Observers League in Japan (VSOLJ), 0061
Kim C.-H., Lee J. W., Kim S.-L., Han W., Koch R. H., 2003, AJ, 125, 322
Koleva M., Prugniel P., Bouchard A., Wu Y., 2009, A&A, 501, 1269
Kurochkin N. E., 1960, Astronomicheskij Tsirkulyar, 212, 9

Liu N. P., 2014, Observations and Studies on K-type Close Binaries, Chinese Academy of Sciences Gradual Thesis, p. 101
Lucy L. B., 1976, ApJ, 205, 208
Luo A.-L. et al., 2015, Res. Astron. Astrophys., 15, 1095
Maceroni C., Milano L., Russo G., 1984, A&AS, 58, 405
Majewski S. R., Zasowski G., Nidever D. L., 2011, ApJ, 739, 25
Menke J., 2005, Information Bulletin on Variable Stars, 5600, 1
Moschner W., 2007, Information Bulletin on Variable Stars, 5761
Nakajima K., 2009, Variable Star Observers League in Japan (VSOLJ), 0048
Nelson R., 2008, Information Bulletin on Variable Stars, 5820
Nelson R., 2009, Information Bulletin on Variable Stars, 5875
Okan A., 2013, Information Bulletin on Variable Stars, 6075
Prugniel P., Soubiran C., 2001, A&A, 369, 1048
Prugniel P., Soubiran C., Koleva M., Le Borgne D., 2007, preprint (astro-ph/0703658)
Qian S., Yang Y., 2005, MNRAS, 356, 765
Qian S.-B., He J.-J., 2005, PASJ, 57, 977
Qian S.-B., Liu L., Soonthornthum B., Zhu L.-Y., He J.-J., 2006, AJ, 131, 3028
Robertson J. A., Eggleton P. P., 1977, MNRAS, 179, 359
Rucinski S. M., 2015, AJ, 149, 49
Szczygieł D. M., Socrates A., Paczyński B., Pojmański G., Pilecki B., 2008, Acta. Astron., 58, 405
van Hamme W., 1993, AJ, 106, 2096
Van Hamme W., Wilson R. E., 2007, ApJ, 661, 1129
Wilson R. E., 1979, ApJ, 234, 1054
Wilson R. E., 1990, ApJ, 356, 613
Wilson R. E., 2008, ApJ, 672, 575
Wilson R. E., 2012, AJ, 144, 73
Wilson R. E., Devinney E. J., 1971, ApJ, 166, 605
Wilson R. E., Devinney E. J., 1973, ApJ, 182, 539
Wilson R. E., Van Hamme W., Terrell D., 2010, ApJ, 723, 1469
Wu Y., Singh H. P., Prugniel P., Gupta R., Koleva M., 2011a, A&A, 525, A71
Wu Y. et al., 2011b, Res. Astron. Astrophys., 11, 924
Wu Y., Du B., Luo A., Zhao Y., Yuan H., 2014, Statistical Challenges in 21st Century Cosmology, IAU Symposium 306, 340
Xiang F. Y., Zhou Y. C., 2004, New Astron., 9, 273
Yakut K., Eggleton P. P., 2005, ApJ, 629, 1055
Yang Y. G., Qian S. B., Gonzalez-Rojas D. J., Yuan J. Z., 2005, Ap&SS, 300, 337
Yuan H. B., Liu X. W., Xiang M. S., 2013, MNRAS, 430, 2188
Zhang J., Qian S.-B., 2013, AJ, 145, 156
Zhang X. B., Zhang R. X., Deng L., 2005, AJ, 129, 979
Zhou X., 2016, The Observation and Investigation on AF-type Contact Binary. Chinese Academy of Sciences Gradual Thesis, p. 78,
Zhou D.-Q., Leung K.-C., 1990, ApJ, 355, 271

This paper has been typeset from a TEX/LATEX file prepared by the author.